Journal of Hydrology xxx (xxxx) xxxx

Contents lists available at ScienceDirect

Journal of Hydrology

journal homepage: www.elsevier.com/locate/jhydrol

Research papers

Conditional mean, effective, and realizations of hydraulic conductivity fields

Xu Gao[a,d], Tian-Chyi Jim Yeh[b,c,*], E-Chuan Yan[a], Yu-Li Wang[b], Yonghong Hao[c]

[a] Faculty of Engineering, China University of Geosciences, Wuhan 430074, China
[b] Department of Hydrology and Atmospheric Sciences, University of Arizona, Tucson, AZ, USA
[c] Key Laboratory for Water Environment and Resources, Tianjin Normal University, Tianjin, China
[d] Engineering Research Center of Rock-Soil Drilling & Excavation and Protection,Ministry of Education, China University of Geosciences, Wuhan 430074, China

ARTICLE INFO

This manuscript was handled by A. Bardossy, Editor-in-Chief

Keywords:
Successive linear estimator
Conditional effective hydraulic conductivity
Conditional hydraulic conductivity realizations
Karhunen-Loeve expansion
Conditional covariance matrix
Uncertainty

ABSTRACT

This study first discusses the conditional mean, realizations, and effective hydraulic conductivity in a theoretical framework. It then introduces Monte Carlo simulation (MCS) algorithms for constraining the outcome by either hydraulic conductivity (K) samples or hydraulic head (h) measurements from the hydraulic tomographic survey (HT). It demonstrates that kriging using K measurements leads to a conditional mean K field, while inverse modeling using successive linear estimator (SLE) with head measurements of HT yields the conditional effective K field. The effects of conditioning using K measurements are different from those using heads. Besides, the conditional effective K leads to the unbiased prediction of the head that honors the observed head at measurement locations. More importantly, the study reveals that the harmonic and geometric means of conditional realizations of K fields of MCS, given head measurements, are equivalent to the conditional effective K in one- and two-dimensional flows, respectively. The first-order approximation in the SLE results in a conditional covariance similar to that from MCS with smaller magnitudes. Despite the difference, all approaches predict unbiased conditional mean head behaviors.

1. Introduction

Interpreting and extrapolating spatial point data to other locations or estimating spatial distributions of hydraulic properties using sparsely observed system responses is a common problem in hydrology, geophysics, and other environmental sciences and engineering fields. For solving these problems, many methods have been developed over the past decades. Among all these methods, kriging is generally a widely used method in the groundwater hydrology field. Similarly, model calibration or inverse modeling is popular for extracting information contained in the responses of aquifers to estimate the spatial distribution of hydraulic parameters (Franssen et al., 2009). While these methods have become routine, the logic behind these approaches, and characteristics of the estimates are unclear, let alone ways to address the uncertainty of these estimates. For these purposes, we focus on the estimates using kriging and hydraulic tomography (HT) and explain conditional mean, realizations, and effective hydraulic conductivity field engrained in these methods.

HT is a new generation of data collection and inverse modeling strategy. Many (e.g.,Tosaka et al., 1993; Gottlieb and Dietrich, 1995) proposed the concept of hydraulic tomography (HT) using pressure variations induced by aquifer pumping to characterize hydraulic property distribution in the aquifer. Yeh and Liu (2000) subsequently developed the first fully 3-D steady-state hydraulic tomography, using a successive linear estimator (SLE)–an inverse algorithm based on the spatial stochastic concept (Yeh et al., 1995, 1996). The accuracy and utility of HT were then tested and verified in sandbox experiments by Liu et al. (2002). Later, Zhu and Yeh (2005) developed the transient hydraulic tomography, and Xiang et al. (2009) expanded SLE to SimSLE (Simultaneous SLE), which simultaneously includes all the pumping test data sets for THT analysis.

Since then, the development and testing of this new technology have thrived. More than two-hundred seventy related research activities and papers have burgeoned since then. Initially, research on hydraulic tomography consisted largely of numerical studies (e.g., Bohling et al., 2002; Brauchler et al., 2003; Zhu and Yeh, 2005, 2006; Ni and Yeh, 2008; Fienen et al., 2008; Castagna and Bellin, 2009; Xiang et al., 2009; Liu and Kitanidis, 2011; Cardiff and Barrash, 2011). These numerical studies are followed by laboratory sandbox and field studies (e.g., Illman et al., 2007, 2009; Liu et al., 2007; Yin and Illman, 2009a, 2009b; Cardiff et al., 2013; Hochstetler et al., 2016; Sanchez-León et al., 2016).

Over the past decades, HT has been analyzed mainly using geostatistical inverse models (such as SLE developed by Yeh et al. (1996) or

* Corresponding author at: Department of Hydrology and Atmospheric Sciences, University of Arizona, Tucson, AZ, USA.
E-mail address: yeh@hwr.arizona.edu (T.-C. Jim Yeh).

https://doi.org/10.1016/j.jhydrol.2020.125606
Received 24 October 2019; Received in revised form 29 September 2020; Accepted 2 October 2020
Available online 08 October 2020
0022-1694/

Quasi-Linear Geostatistical Approach (QLGA) developed by Kitanidis (1995). Other approaches have also been used: the pilot point method (e.g., Castagna and Bellin (2009); Lavenue and Marsily (2001)), a low-frequency asymptotic approach by Vasco and Karasaki (2006), and ray tracing methods (e.g., Brauchler et al., 2007). These algorithms focus on estimating smooth fields except the recent application of ensemble Kalman Filters (ENKFs) to HT by Schöniger et al. (2012). Recognizing the stochastic nature of the inverse modeling, Nowak (2009) advocated the benefits of empirical cross-covariances from Monte Carlo (MC) analyses in the ENKFs.

In this paper, we first use a stochastic formulation to articulate conditional mean, effective, and realizations of hydraulic conductivity (K) and head fields. We then introduce kriging, which estimates the conditional mean K field, and the KSA (kriging with a superposition approach), and the Karhunen-Loeve expansion method (KLM), which derive conditional realizations of K fields, conditioned on the K measurements. Afterward, the successive linear estimator (SLE), which derive the effective K field, conditioned on some observed heads, is discussed. Subsequently, the Monte Carlo SLE (SLEMCS) and SLE with KLM (SLEKLM) approaches for generating conditional realizations of K fields, which honor the observed heads, are proposed. We then apply these techniques to one- and two-dimensional numerical experiments to corroborate the results of the stochastic theories.

2. Theories

Before discussing the stochastic theories, we assume that the following equations describe the steady-state flow field due to pumpings in a saturated heterogeneous porous media:

$$\nabla\cdot[K(\boldsymbol{x})\nabla H(\boldsymbol{x})] + Q(\boldsymbol{x}) = 0 \tag{1}$$

with boundary conditions

$$H|_{\Gamma 1} = H_1,\ [K(\boldsymbol{x})\nabla H(\boldsymbol{x})]\cdot\boldsymbol{n}|_{\Gamma 2} = q \tag{2}$$

In Eq. (1), H is the total head [L]; $\mathbf{x}$ is the location vector [L], Q is the pumping rate [1/T]; K is hydraulic conductivity [L/T]. In Eq. (2), H_1 is the prescribed total head on the Dirichlet boundary Γ_1 and specific discharge q [L/T] is specified on the Neumann boundary conditions Γ_2 $\boldsymbol{n}$ is a unit vector normal to Γ_2.

2.1. Unconditional realizations and effective K

Investigation of effects of imposing hydraulic conductivity (K) and head (H) on the analysis and simulation of groundwater flow in aquifers is most appropriate to formulate the problem in a stochastic framework and to consider a pumping test at a single well. The discussion starts with the case where no point data can be used to condition the hydraulic conductivity or the resulting head fields.

Since $K(\boldsymbol{x})$ is spatially varying and challenging to determine it at every location of the aquifer, the stochastic analysis conceptualizes K as a random field:

$$K(\boldsymbol{x}, \omega) = \bar{K} + K'(\boldsymbol{x}, \omega) \tag{3}$$

where $\bar{K}$ is the unconditional mean (the arithmetic average of all possible K realizations), which are invariant in the spatial and ensemble. The overhead bar stands for the expected value. The unconditional perturbations at each $\mathbf{x}$ are $K'(\boldsymbol{x}, \omega)$, where ω is the ensemble realization index ($\omega = 1, \ldots\infty$), which are characterized by their unconditional covariance function. This covariance specifies the spatial variance, the uncertainty of the perturbations, and the spatial relationship between perturbations in the ensemble sense or the spatial sense if the spatial domain is sufficiently large (i.e., ergodicity is met).

Accordingly, many possible steady head fields $H(\boldsymbol{x}, \omega)$ exist in this aquifer induced by a pumping test with a given Q. These fields are thus a random field:

$$H(\boldsymbol{x}, \omega) = \bar{H}(\boldsymbol{x}) + H'(\boldsymbol{x}, \omega) \tag{4}$$

in which $\bar{H}(\boldsymbol{x})$ is the unconditional ensemble mean, which varies with $\mathbf{x}$ and $H'(\boldsymbol{x}, \omega)$ is the perturbation at $\mathbf{x}$.

Substituting Eqs. (3) and (4) into the governing flow equation Eq. (1), we have

$$\nabla\cdot[(\bar{K} + K'(\boldsymbol{x}, \omega))\nabla(\bar{H}(\boldsymbol{x}) + H'(\boldsymbol{x}, \omega))] = Q \tag{5}$$

Monte Carlo simulation is one way to derive the possible head fields corresponding to all possible K fields. Averages of these fields over the ensemble are their means, and their variances represent deviations of the means from the true fields.

Instead of all possible $H(\boldsymbol{x})$ fields, we can seek the unconditional mean of $H(\boldsymbol{x}, \omega)$ directly. To do so, we expand Eq. (5) and take the expected value of Eq. (5) to derive an unconditional mean flow equation:

$$\nabla\cdot(\bar{K}\,\nabla\bar{H}(\mathbf{x})) + \nabla\cdot(\overline{K'(\boldsymbol{x}, \omega)\nabla H'(\boldsymbol{x}, \omega)}) = Q \tag{6}$$

which can also be rewritten as:

$$K_{eff}\,\nabla^2\bar{H}(\boldsymbol{x}) = Q_0 \tag{7}$$

The term $K_{eff} = \bar{K} + \nabla\cdot(\overline{K'(\boldsymbol{x}, \omega)\nabla H'(\boldsymbol{x}, \omega)})[\nabla^2\bar{H}(\boldsymbol{x})]^{-1}$ is the unconditional effective parameter. K_{eff} is often assumed to be invariant in ensemble and space, while some analysis (e.g., Indelman, 2003) showed that it varies with radial distance near the pumping well and then approaches some constant values at large radial distances. Nevertheless, this K_{eff} yields the ensemble mean of $H(\boldsymbol{x}, \omega)$ field under all possible heterogeneity, given the pumping discharge. Then, the unconditional variance of $H'(\boldsymbol{x}, \omega)$ (Gelhar, 1986) quantifies the deviation of $H(\boldsymbol{x}, \omega)$ from $\bar{H}(\boldsymbol{x})$.

2.2. Conditional realizations and mean K with K samples

Suppose we know the K values at some sampling locations $\mathbf{x}$s, and we like to use them for mapping the K distribution of an aquifer to increase the prediction accuracy of the flow field. A conditional approach is appropriate, which requires a highly parameterized model and K fields that are consistent with the measured K values at the sampling locations. For this purpose, we formulate a condition flow equation:

$$\nabla\cdot[(\bar{K}_c(\boldsymbol{x}) + K_c'(\boldsymbol{x}, \omega))\nabla(\bar{H}_c(\boldsymbol{x}) + H_c'(\boldsymbol{x}, \omega))] = Q \tag{8}$$

where the subscript c denotes "conditioned." Eq. (8) is the governing equation for the flow in realizations of K fields conditioned on the K samples. Notice that the K samples implicitly condition the head. Eq. (8) can serve as the equation in which flow is conditioned on the head measurements (to be discussed in Section 2.3.)

Solving Eq. (8) using conditional realizations of K fields, $\bar{K}_c(\boldsymbol{x}) + K_c'(\boldsymbol{x}, \omega)$, yields many realizations of heads $\bar{H}_c(\boldsymbol{x}) + H_c'(\boldsymbol{x}, \omega)$, which reflect the effects of conditioning by the K samples. Notice that $\bar{K}_c(\boldsymbol{x})$ and $K_c'(\boldsymbol{x}, \omega)$ represent the conditional mean and perturbation of K, respectively, while $\bar{H}_c(\boldsymbol{x})$ and $H_c'(\boldsymbol{x}, \omega)$ are the conditional mean and perturbations of heads, respectively. Implementation of this solution requires one to generate all possible K field conditioned on the K samples, using KSA or KLM methods (Section 3) first and then solves the equation for all conditional head fields. This procedure is called the conditional Monte Carlo simulations (conditional MCS). The average of all conditional K fields from MCS results in the conditional mean K field, while the average of all the simulated head is the conditional mean head field, given the K samples.

Alternatively, one can expand Eq. (8) and take its expected value to have

$$\begin{aligned}\nabla\cdot[(\bar{K}_c(x)\nabla\bar{H}_c(x) + \cancel{\overline{K_c'(x, \omega)}\nabla\bar{H}_c(x)})\\ + \nabla(\cancel{\bar{K}_c(x)\nabla\overline{H_c'}(x, \omega)} + \overline{K_c'(x, \omega)\nabla H_c'(x, \omega)})] = Q\end{aligned} \tag{9}$$

Recognizing the expected value of the product of a perturbation and a mean of a variable is zero (the cross-out terms). We then normalize $K_c'(\boldsymbol{x}, \omega)\bar{\nabla}H'(\boldsymbol{x}, \omega)$ with the mean flux $\bar{K}_c(\boldsymbol{x})\nabla\bar{H}_c(\boldsymbol{x})$, and lump the normalized cross-covariance with $\bar{H}_c(\boldsymbol{x})$, one has

$$\nabla\cdot[\bar{K}_c(\boldsymbol{x})\nabla < \bar{H}_c(\boldsymbol{x})(1 + K_c'(\boldsymbol{x}, \omega)\bar{\nabla}H_c'(\boldsymbol{x}, \omega)[\bar{K}_c(\boldsymbol{x})\nabla\bar{H}_c(\boldsymbol{x})]^{-1}) >] = Q$$

or

$$\nabla\cdot[\bar{K}_c(\boldsymbol{x})\nabla(H_{ceff}(\boldsymbol{x}))] = Q \tag{10}$$

which is the conditional mean equation in which $\bar{K}_c(\boldsymbol{x})$ is the conditional mean K from kriging. That is to say, if we use the condition mean K field to solve the flow equation, we directly obtain the conditional effective head field H_{ceff}. However, this head field is not the conditional mean head field from the MCS approach.

To derive the conditional mean head, one can group the normalized covariance with $\bar{K}_c(\boldsymbol{x})$. That is,

$$\nabla\cdot[\bar{K}_c(\boldsymbol{x})\langle(1 + K_c'(\boldsymbol{x}, \omega)\bar{\nabla}H_c'(\boldsymbol{x}, \omega)[\bar{K}_c(\boldsymbol{x})\nabla\bar{H}_c(\boldsymbol{x})]^{-1})\rangle\nabla\bar{H}_c(\boldsymbol{x})] = Q \text{ or}$$

$$\nabla\cdot[\bar{K}_{ceff}(\boldsymbol{x})\nabla(\bar{H}_c(\boldsymbol{x}))] = Q \tag{11}$$

Solving Eq. (11) with $\bar{K}_{ceff}(\boldsymbol{x})$ yields the conditioned mean head, given the K samples, which is identical to the conditioned mean head from MCS. This approach, however, requires $K_c'(\boldsymbol{x}, \omega)\bar{\nabla}H_c'(\boldsymbol{x}, \omega)$ to be known beforehand.

2.3. Conditional realizations and effective K with head measurements

Similar to using K measurements to condition the simulated head field, this conditional head approach also adopts a highly parameterized conceptual model. The governing equation is identical to Eq. (8) but is for the flow in realizations of unknown K fields conditioned on the head samples. That is, the mean and perturbation of K and head in Eq. (8) are conditioned on the head measurements, instead of the sampled K.

To determine these realizations of unknown K fields, we need to solve an inverse problem using some algorithms (Section 3), which can select all possible realizations of K fields with which the groundwater flow model can reproduce the observed heads at the monitoring locations. In other words, a conditional MCS using SLEMCS or SLEKLM algorithm (see Section 3) is necessary. Once all possible realizations of K and H fields are obtained, their average leads to the conditional mean K and H fields, respectively.

Instead of using the MCS, most inverse modeling efforts have attempted to seek one possible of K field that can preserve the observed heads when the flow equation is solved. To explain the theory, we make the use of Eq. (11) as the conditional mean equation, but recognize the equation is conditioned on the observed head, rather than the K measurements. In this mean equation, $\bar{K}_{ceff}(\boldsymbol{x})$ and $\bar{H}_c(\boldsymbol{x})$ are the conditional effective hydraulic conductivity and conditional mean heads, given the head observations. Solving the conditional mean equation to match the observed head in a least-square sense using an algorithm such as SLE (Section 3), one has the conditional mean head and the effective K field. While the effective K is not necessarily the same as the arithmetic mean of all possible conditional realizations of K fields, it produces the conditional mean head, which is unbiased and preserves the observed heads.

3. Methods

To substantiate the above theories, we introduce several methods that derive the conditional mean and realizations of K fields, given some K samples. We also present methods for deriving conditional effective K and condition realizations of K, given some observed heads.

3.1. Conditional mean K field with K samples

Kriging is a widely accepted method to derive the conditional mean K field, given the sampled K values. Readers are referred to the description of kriging in textbooks, such as Kitanidis (1997) and many

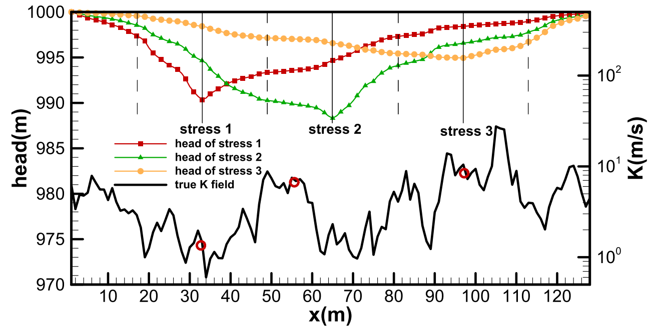

Fig. 1. The true K distribution (red circles denote K sampling locations) along a one-dimensional horizontal confine aquifer, and the true steady-state head distributions during the three stresses of HT.

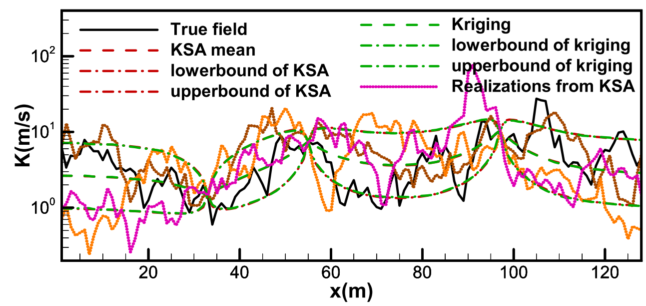

Fig. 2. Comparisons of the true, the kriged, the KSA (mean of the conditional realizations) hydraulic conductivity field, and selected conditional K realizations. Upper and lower bounds are the conditional standard deviation of kriging estimates and that from conditional realizations using kriging superposition approach (KSA).

others.

3.2. Conditional K realizations with K samples

Kriging Superposition Approach (KSA). To create conditional realizations, given some K measurements, we use a Monte Carlo simulation algorithm based on superposition (e.g., Yeh, 1992). It consists of four steps. **Step 1:** Use the natural logarithm of K (ln$K$ or Y) to avoid negative estimated values and generate a conditional mean ln$K$ field ($Y_c(\bar{\boldsymbol{x}}, f)$, where f denotes the given field data) using kriging and measured lnK^* at measurement locations. **Step 2:** Generate k realizations of the unconditional random field $Y(x, \omega)$ (where ω is the realization index, $\omega = 1, \ldots k$) via a random field generator (e.g., Gutjahr (1989)) with a known mean, variance, and autocorrelation distances. **Step 3:** Extract the ln$K$ values from $Y(x, \omega)$ at the same sample locations as those at the field site. Then, use these sample values and kriging in Step 1 to calculate corresponding conditional mean fields, $Y_c(\bar{\boldsymbol{x}}, \omega)$, $\omega = 1, \ldots k$, given these generated samples. Next, we determine the difference between each generated random field and its associated conditional mean field. This is,

$$D(x, \omega) = Y(x, \omega) - Y_c(\bar{x}, \omega) \tag{12}$$

Step 4: Add the differences in Eq. (12) to the conditional mean Y of the field site from step 1 to derive the conditional realizations:

$$Y_c(x, \omega) = Y_c(\bar{x}, f) + D(x, \omega) \tag{13}$$

These conditional realizations thus preserve the sample values at the sample locations of the field site since $D(x, \omega) = 0$ at these locations. At other locations, $Y_c(x, \omega)$'s are random variables determined by deviations $D(x)$ and kriging estimates based on the field observations.

Karhunen-Loeve Expansion Method (KLM). In this method, $\mathbf{Y}_c(\boldsymbol{x}, \omega)$, can be written as,

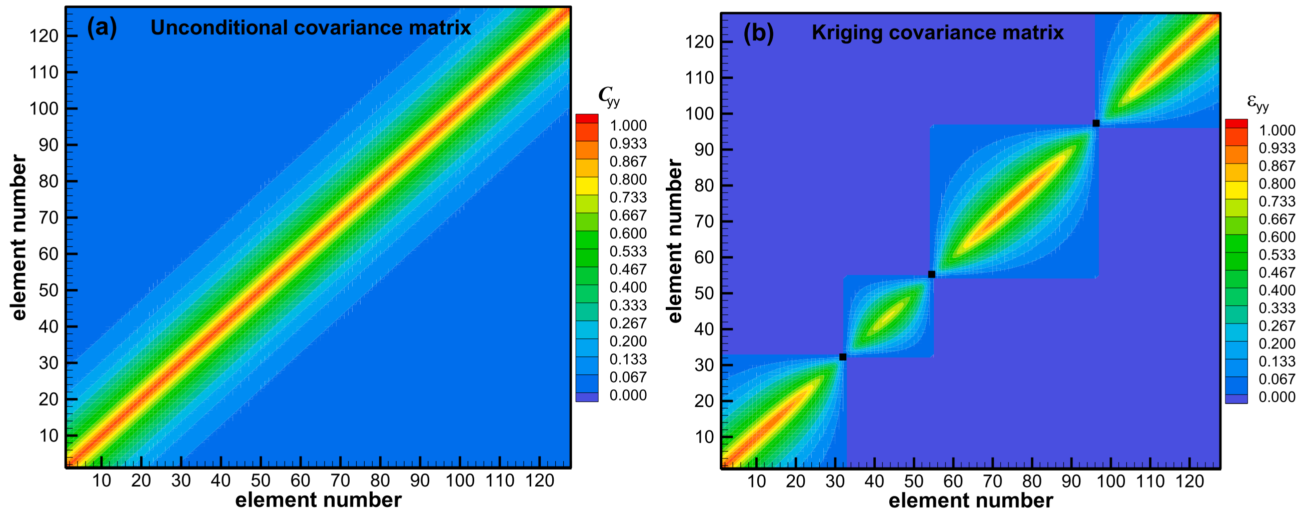

Fig. 3. (a) Unconditional covariance matrix of ln*K*; (b) kriging conditional covariance matrix of ln*K* (the solid squares denote the *K* sample locations).

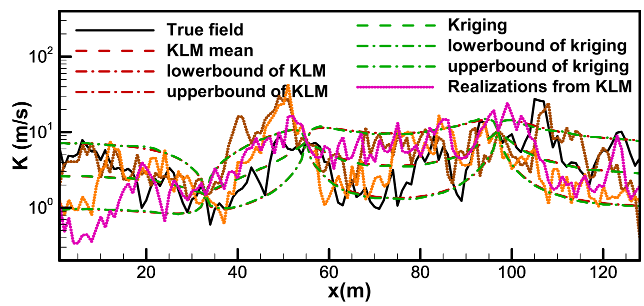

Fig. 4. Comparisons of kriging estimates and associated conditional standard deviation of *K* with the conditional random field of case 1 (i.e., *K* measurements only) by using the Karhunen-Loeve expansion method (KLM).

$$\boldsymbol{Y_c}(\boldsymbol{x}, \omega) = \boldsymbol{Y_c}(\bar{x}, \omega) + \xi\sqrt{\lambda}\,\boldsymbol{g} \tag{14}$$

where $\boldsymbol{Y_c}(\bar{x}, \omega)$ is the conditional mean *K* derived from kriging or the effective *K* from SLE. The last term in the Eq. (14), $\xi\sqrt{\lambda}\boldsymbol{g}$, is the perturbation term, and $\boldsymbol{\xi}(n_y \times 1)$ are a set of uncorrelated random variables with zero mean and unit variance, i.e., $\bar{\xi_i} = 0$, $\bar{\xi_i\xi_i} = 1$, and $\bar{\xi_i\xi_j} = 0$, when $i \neq j$. Furthermore, $\mathbf{g}(n_y \times \infty)$ are orthogonal eigenvectors. $\boldsymbol{\lambda}(\infty \times \infty)$ is a diagonal matrix filling with corresponding nonnegative eigenvalues. Based on the conditional covariance function, the eigenvalues and eigenvectors are obtained by eigenvalue decomposition of the conditional covariance $\boldsymbol{\Lambda}_{yy}$ from kriging:

$$\Lambda_{yy} = g^T\lambda g \tag{15}$$

The decomposition is easily accomplished by the built-in *eig* function in MATLAB, in which the *eig* function will automatically select the Cholesky factorization algorithm to compute the $\boldsymbol{\lambda}$ and $\mathbf{g}$ since the conditional covariance matrix is Hermitian (Ma, Dong, and Zhang, 2006; MathWorks, 2005; Yaz and Azemi, 1995). Afterward, we sort the eigenvalues in the descending order. Then, only the n_y eigenvalues and the associated eigenvectors are retained to approximate the perturbation term in Eq. (14). That is, the dimensions of matrix $\boldsymbol{\lambda}$ and $\mathbf{g}$ in the truncated KL expansion are reduced to $n_y \times n_y$. At last, with given different random variables vectors $\boldsymbol{\xi}(n_y \times 1)$, different random fields are generated. Note that Lu and Zhang, (2004) derived a solution for eigenvalue decomposition in KL expansion, which is different from our method.

3.3. Conditional effective K field with head data

While many different inverse methods could be used for this purpose, we focus on HT estimates using the successive linear estimator (SLE), Yeh et al. (1996), which has widely used as we mentioned in the introduction.

Suppose we collect n_d observed heads in space, denoted by the data vector $\mathbf{d}^*$ during a steady-state HT survey. The conditional effective $\boldsymbol{Y_{ceff}}(\boldsymbol{x})$ with given observations is determined using the following SLE:

$$\boldsymbol{Y_{ceff}}(\boldsymbol{x})^{(r+1)} = \boldsymbol{Y_{ceff}}(\boldsymbol{x})^{(r)} + \omega^{\mathrm{T}}(\boldsymbol{d}^* - \boldsymbol{d}^{(r)}) \tag{16}$$

where r is the iteration index; the vector $\mathbf{d}^{(r)}$ is the simulated heads at the observation locations obtained from the forward model (i.e., Eqs. (1) and (2)), using $\boldsymbol{Y_{ceff}}(\boldsymbol{x})$ at iteration r. When $r = 0$, $\boldsymbol{Y_{ceff}}(\boldsymbol{x})$ is the unconditional mean. The coefficient matrix, $\boldsymbol{\omega}$ $(n_d \times n_y)$, denotes the weights, which assign the contribution of difference between the observed and simulated head at each observation location to the previously estimated $\boldsymbol{Y_{ceff}}(\boldsymbol{x})$ field, and the superscript T denotes the transpose. This coefficient matrix $\boldsymbol{\omega}$ is derived by solving the following equations:

$$[\varepsilon_{dd}^{(r)} + \theta^{(r)}\mathrm{diag}(\varepsilon_{dd}^{(r)})]\,\omega^{(r)} = \varepsilon_{dy}^{(r)} \tag{17}$$

where ε_{dd} is the covariance of the head, and ε_{dy} is the cross-covariance between ln*K* and head. The parameter θ is a dynamic stability multiplier, and $\mathrm{diag}(\varepsilon_{dd})$ is a stability factor, which is a diagonal matrix with the same diagonal elements as ε_{dd}. The covariance ε_{dd} and cross-covariance ε_{dy}, can be derived from the first-order numerical approximation (e.g., Yeh and Liu, 2000):

$$\begin{aligned} \varepsilon_{dd}^{(r)} &= \boldsymbol{J}_d^{(r)}\varepsilon_{yy}^{(r)}\boldsymbol{J}_d^{(r)\mathrm{T}}, \\ \varepsilon_{dy}^{(r)} &= \boldsymbol{J}_d^{(r)}\varepsilon_{yy}^{(r)} \end{aligned} \tag{18}$$

where $\mathbf{J}_d$ $(n_d \times n_y)$ is the sensitivity (Jacobian) matrix of head data with respect to ln*K* using the ln*K* estimated at the current iteration. At iteration $r = 0$, the $\varepsilon_{yy}(n_y \times n_y)$ is the unconditional covariance of ln*K*. For $r \geq 1$ the conditional or conditional covariance function are evaluated according to

$$\varepsilon_{yy}^{(r+1)} = \varepsilon_{yy}^{(r)} - \omega^{\mathrm{T}}\varepsilon_{dy} \tag{19}$$

The above steps (Eq. (16) through Eq. (19)) are repeated until the convergence of the solution is achieved. One convergence criterion is the change in variances of the estimated ln*K* field between the current iteration and the previous iteration. If this criterion is small, SLE cannot improve the estimates any further. The other is the change of simulated heads between successive iterations. If this quantity is small, the estimates could not further fit the observed heads. Once one of the two criteria is met, we consider the estimates to be optimal, and we terminate the iteration.

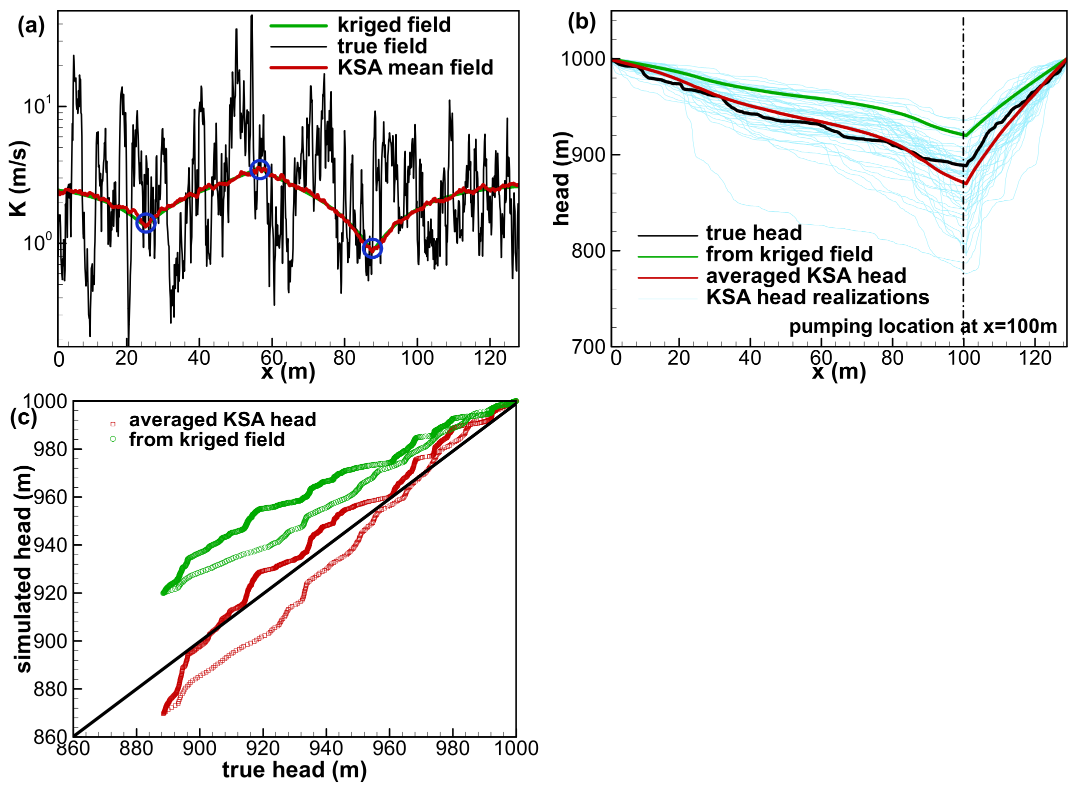

Fig. 5. (a) Comparisons of the true, the kriged, the KSA mean of hydraulic conductivity field with 1024 elements (The blue circles denote the sampled locations). (b) Head simulations from the true field, kriging field, and KSA conditional random fields. (c) Scatter plot of true head vs. simulated head from the kriged field and averaged KSA head.

The above algorithm can be applied to each pumping test in HT survey sequentially SSLE (Sequential SLE, Zhu and Yeh (2005)) or all the pumping tests simultaneously (Simultaneous SLE, Xiang et al. (2009)).

3.4. Conditional K realization with head data

MCS using SLE (SLEMCS). Besides the conditional effective hydraulic conductivity field, SLE can generate many possible realizations of $\boldsymbol{Y_c}(\boldsymbol{x}, \omega)$ fields that preserve the observed head, and satisfy their underlying statistical properties (i.e., mean and covariance) as well as the governing flow equation (Eqs. (1) and (2)). Similar to the approach proposed by (Gutjahr et al., 1994; Hanna and Yeh, 1998), one way for this purpose is the Monte-Carlo simulation (SLEMCS), as described below.

This approach uses an unconditional realization K field as the starting field, and its unconditional covariance is employed as the prior covariance for SLE. Then, SLE iteratively updates the estimates and conditional covariance until the simulated heads agree with the observed ones. Once the estimated field converges, the estimated ln$K$ field becomes the conditional realization given head measurements of HT survey. If we repeat this procedure with other unconditional realizations, we then have a conditional MC simulation for HT.

This approach is analogous to the iterative ENKFs (Nowak, 2009; Schöniger et al., 2012), but it uses sensitivity and the first-order analysis to update the conditional covariances as opposed to calculating the conditional covariances using the approximated conditional realizations during each iteration.

MCS using KLM (SLEKLM). As an alternative to SLEMCS, SLEKLM takes advantage of the effective ln$K$ field and the conditional covariance (ε_{yy}) from SLE, and then directly uses KLM to generate conditional realizations. That is, KLM generates zero mean realizations based on the ε_{yy} at the final iteration from SLE, which are then added to the effective ln$K$ field from SLE to produce the conditional realizations. This approach thus avoids the time-consuming conditioning MC simulation based on SLE as in SLEMCS approach.

4. One-dimensional numerical experiments

4.1. Case I: Conditioning using K measurements

For the sake of easy visualization and understanding, we use a one-dimensional confined aquifer to demonstrate the algorithms above. This aquifer is 128 m in length and is discretized into 128 elements (each 1 m) and 129 nodes. Each element is assigned a K value from a Fast Fourier Transform (FFT) random field generator (Gutjahr, 1989). The generation assumes that the ln$K$ has a jointly normal distribution with a mean of 1.0, a variance of 1.0 and an exponential correlation structure whose correlation scale equals to 10 m. This K field is depicted in Fig. 1 as the solid black line, and the unit of K is m/s. The K values at x = 32, 56, and 96 are taken as the hydraulic conductivity measurements (red circles in the figure) so that there are 125 unknowns of K. Using three K samples and the exact spatial statistics, we derive the conditional mean K field, via kriging, and conditional realizations of K fields, through KSA and KLM, given the three sample values.

Kriging. The conditional mean K field derived by kriging using three K samples is displayed as a green long-dashed line in Fig. 2. This figure also shows the upper and lower bounds of the kriging estimates (i.e., the conditional mean values plus or minus one standard deviation of the kriging), respectively.

KSA. The dotted color lines in Fig. 2 are three realizations from the 2,000 realizations generated from KSA. Means and standard deviations of the realizations at each location are used to determine the upper and the lower bounds. We observe that these means and the upper and lower bounds agree with the conditional mean and the upper and lower bounds derived from kriging mean and variance.

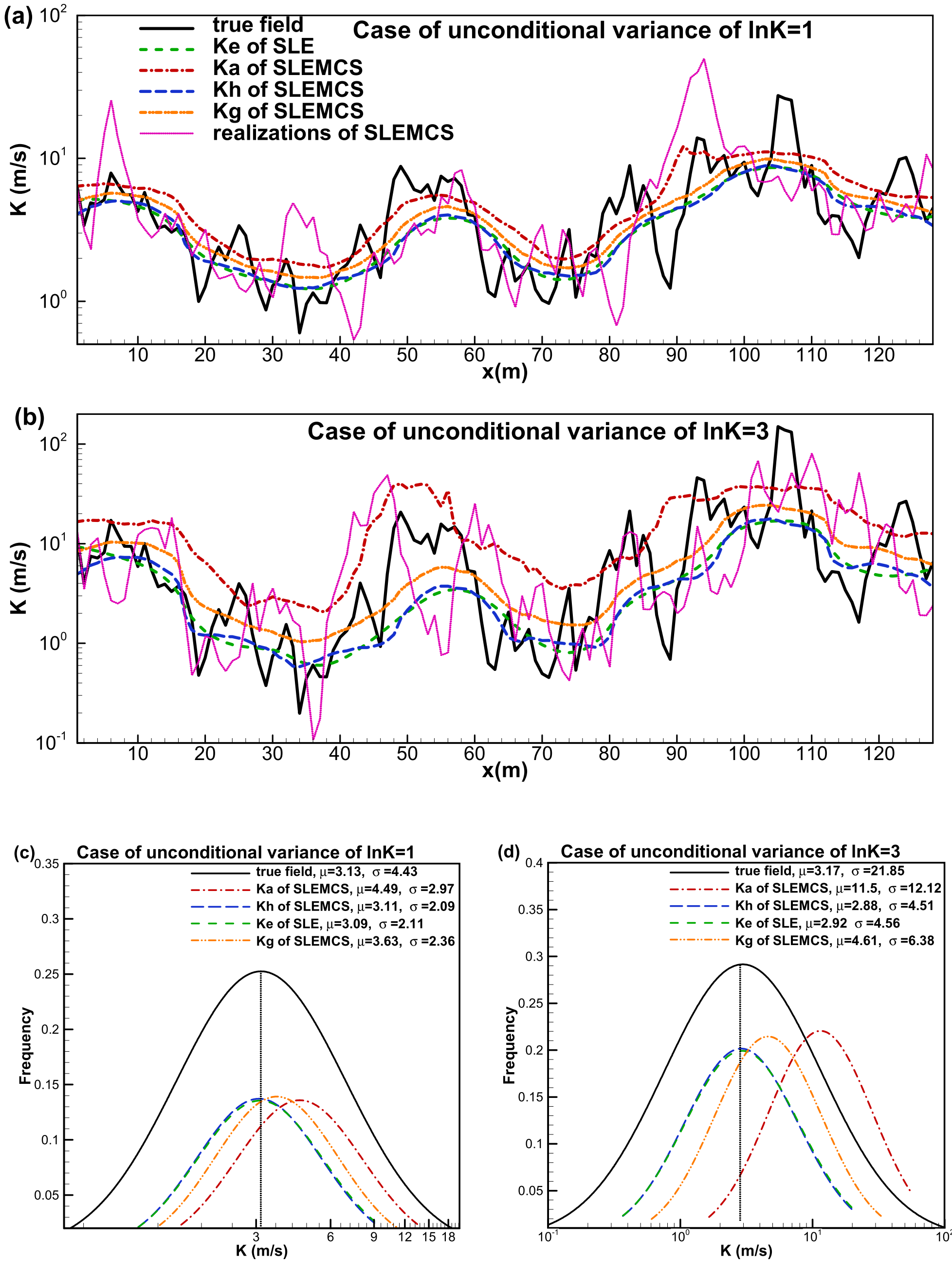

Fig. 6. Conditional effective K from SLE (K_e), the arithmetic (K_a), harmonic (K_h), and geometric mean (K_g) of the conditional Monte Carlo realizations using SLEMCS, true field, and a realization of the SLEMCS: (a). for the unconditional variance of ln$K$ = 1 (i.e., Var_ln$K$ = 1); (b). for the unconditional variance of ln$K$ = 3.0 (i.e., Var_ln$K$ = 3). Figures (c) and (d) are the histogram, mean and standard deviations of these fields for Var_ln$K$ = 1 and 3, respectively.

From Fig. 2, we observe 1) the conditional means at the sample locations are identical to the values of the samples, 2) the conditional mean K captures the general spatial trend of the true ln$K$ field, and 3) the closer the location to sampled locations (say, less than 10 m), the smaller fluctuations of the ln$K$ values of the realization. We also observe that the smaller the distance to the sample location, the narrower the gap between the upper and lower bounds. This result indicates that the measurements have strong influences on the K at distances less than 10 m (the correlation scale of the heterogeneity) from the sampling locations. Beyond this distance, the mean values remain the same as the unconditional mean value. In other words, the uncertainty of the true field around the conditional mean at these locations remains the same as the variability of ln$K$ (i.e., effects of conditioning are zero).

The unconditional covariance and the kriging (or conditional) covariance matrices for this problem are exhibited in Fig. 3a and b, respectively. For the unconditional case, the covariance decays rapidly from the diagonal terms according to the correlation scale. The kriging (i.e., conditional) covariance forms four distinct zones according to the three sample locations, and in other areas, the covariance is zero due to zero variance at the sample locations.

KLM. In this approach, the conditional covariance matrix from kriging is directly used in KLM to generate 2,000 realizations of conditional ln$K$ fields. Three of the 2,000 realizations and the true K field are illustrated in Fig. 4. Notice that the realizations are different from those in Fig. 2, generated with KSA because a different random field generator is used. Nevertheless, the conditional means and the upper and the lower bounds of the realizations from KLM are comparable to those derived from KSA. Besides, these realizations from KLM honor the

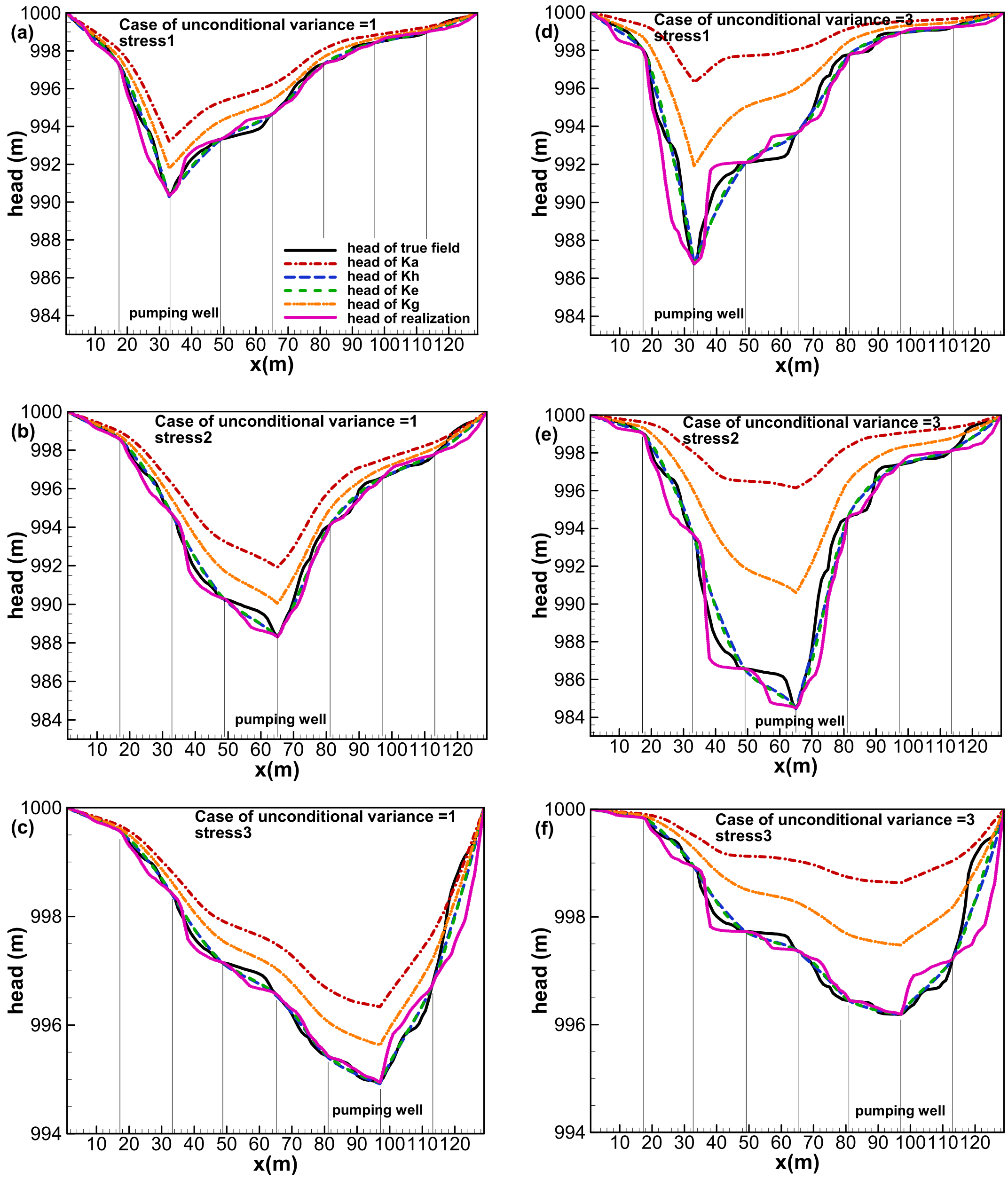

Fig. 7. The simulated head distributions for the three stresses using the effective *K*, and harmonic, arithmetic, and geometric means of *K*, and one realization of *K* from MCS, as well as those from the true *K* field, are shown. Left column, a, b, and c is for Var_ln*K* = 1, and the right (d, e, and f) is for Var_ln*K* = 3. Each predicted head distributions *K* fields are based on the calibration of the stresses.

sample values at sample locations.

In summary, kriging estimates are conditional means of all the possible realizations in the ensemble; they are the means of all the equally likely realizations, which agree with the sample values at the sample locations. Kriging estimates are smoother than the true field since they represent the most likely estimates at the locations where no samples are available, and they are the sample values at the sampled locations. Kriging variance is the statistics that describe the likely deviation of the true field from the conditional means. Notice that if samples are taken at every location, the conditioning means are identical to the true field, and the kriging variance or conditional variance is zero everywhere.

KSA and KLM generate conditional realizations, which have the same spatial statistics (spatial variability) of the true field and honor the sample values at the sample locations. They are as jagged as the true field, but their ensemble averages are similar to the kriging means.

Conditioned Head Fields. To illustrate the effects of conditional mean *K* field from kriging and conditional realizations of KSA on the prediction of head distributions, we create a new 1-D aquifer, which has 1,024 elements (each 0.125 m) with random *K* values with the same length of the aquifer and spatial statistics as in Fig. 1 and bounded by constant heads of 1000 m on the both sides. We increase the number of element of the aquifer to avoid the ergodicity issue. Fig. 5a is an illustration of the *K* field and those from kriging and the average of KSA realizations given the *K* values at three locations. It shows that the kriging mean is identical to the conditional mean of KSA as they should be.

We then simulate the steady head fields due to pumping at a location with a rate of 0.1 m^3/s. In Fig. 5b, the simulated head from the kriged field is consistently higher than the true head of the heterogeneous aquifer, while the average of the simulated conditional head fields (light blue lines in the figure) from conditional 1,000 realizations

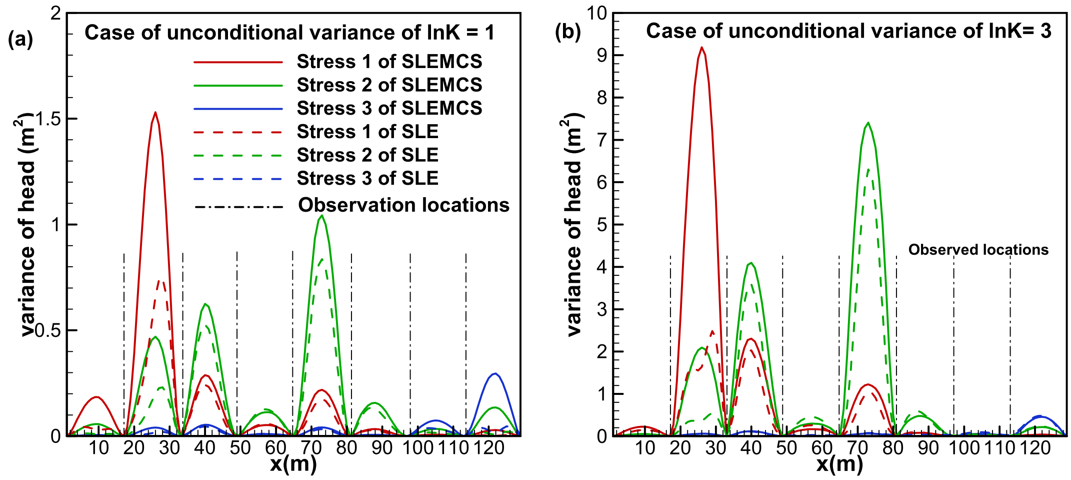

Fig. 8. Conditional head variances between the first-order analysis in SLE (the dashed lines) and those from MCS simulations (the solid lines) for the Var_ln$K$ = 1.0 (a) or 3.0 (b).

of K fields based on KSA is close to the true field. The scatter plots of the simulated head from the kriged K field and that from KSA vs. the true field (Fig. 5c) also confirms that the kriged K field produces the conditional effective head field and that KSA can yield the conditional mean head field, as we have remarked in Section 2.2. The results of KLM are identical to those of KSA and are not presented. However, we cautiously point out that the unbiased prediction could vary with the pumping location, in particular in 1-D aquifers since flow process ergodicity should also be met (Yeh et al., 2015) because the heterogeneity near the pumping well heavily controls the behavior. That is, the unbiased prediction will always be true in the average sense over a larger number of pumping tests at different locations.

4.2. Case II: Conditioning using head data

In this case, two aquifers are considered (AQ1 and AQ2 with an unconditional variance of ln$K$ = 1, and 3, respectively), which have the same mean, correlation scale, and random seed number as that in Case I. The true K fields of the two aquifers are given in Fig. 6a and 6b, which are bounded by the left-hand and right-hand prescribed head boundaries of 1000 m. Seven wells are located at x = 16, 32, 48, 64, 80, 96, and 112 m of the aquifers. Three pumping stresses are conducted at x = 32, 64, and 96 individually as the HT survey, with a constant discharge ($Q = 0.02m^3/s$). We then use VSAFT2 (Yeh et al. 1993), available at *hptt://tian.hwr.arizona.edu/download*, to simulate the steady-state flow field induced by each test, and take the heads at the other six wells for HT analysis. The red, the green, and the orange dotted line in Fig. 1 are the simulated head field in AQ1 for stresses 1, 2, and 3, respectively (the head in AQ2 is not shown).

Using head measurements from the six wells during each test, we derive the most likely effective hydraulic conductivity using SLE without any K measurements. Then, with the same head measurement locations, SLEMCS derives 2,000 equally likely hydraulic conductivity realizations that preserve the observed heads, and so does SLEKLM. The conditional mean and covariance of these K realizations are then calculated to compare with that directly from SLE. The results of this analysis are given below.

4.2.1. SLEMCS

Conditional *K* fields. As shown in Fig. 6a and 6b, the conditional effective K field from SLE captures the spatial trend of the true K field but is smoother than the true field. On the other hand, the conditional realizations from SLEMCS are as erratic as but different from the true field, although with a similar trend. We also see that the harmonic mean of the conditional K realizations agrees with the conditional effective K, while the arithmetic and the geometric mean of the realizations are consistently higher. Comparison of Fig. 6a and 6b indicates that deviations of the arithmetic and geometric means from the effective K increase as the unconditional variance of ln$K$ increases.

The histogram plots in Fig. 6c and 6d show that the distributions of the true field, conditional effective K, and K fields from different averages are log-normal. Notice that the distributions of the effective K field and the harmonic mean of SLEMC are identical, and they have similar means as the true field but smaller variances, reflecting effects of conditioning (i.e., the posterior distribution in Bayesian theory).

These findings corroborate with the fact that 1) SLE produces the conditional effective hydraulic conductivity field, as stated in Yeh et al. (1996), and 2) the effective K in one-dimensional flow scenarios is the harmonic average of all possible conditional realizations (see Yeh et al., 2015).

Conditional head fields. To check if the conditional head fields honor the observed heads, we simulate head fields corresponding to the three pumping tests, using the 2,000 conditional random K fields from SLEMCS, and calculate the conditional means and variances. Note that the SLE approach substitutes the final conditional covariance of ln$K$ (ε_{yy}) into Eq. (18) to determine the conditional head covariance ε_{dd} in which the diagonal elements are its conditional variances.

According to Fig. 7a-c effective K, conditional K realizations and harmonic mean K from SLEMCS yield head fields that honor the observed heads of each stress. They are unbiased estimates of the true head field for each stress even if the unconditional variance of ln$K$ is 3.0 (Fig. 7d-f). Notice that we present only one realization of heads corresponding to one conditional K realization (dotted pink line) in Fig. 7 since other realizations behave similarly. On the contrary, we observe that the arithmetic and geometric means of the conditional K realization form SLEMCS result in heads, departing from the observed, with increasing deviations with the variance of ln$K$. These findings manifest that the effective K is not equal to the ensemble (arithmetic) average of the conditional realizations of K, but is their harmonic average.

The conditional head variances from SLE and SLEMCS are depicted in Fig. 8a for the unconditional variance of ln$K$ = 1; those for the variance equal to 3 are in Fig. 8b. These figures indicate that the conditional variance of the head at each observation location is zero, while the other locations are not. The conditional variances of the head from SLEMCS are larger than those from the first-order analysis used in SLE, and the difference increases with the unconditional variance of ln$K$. These results indicate that the head variances approximated by the first-order analysis in SLE underestimate the conditional variances of the head.

Conditional Covariance of ln*K*. In the case of SLE, the first-order

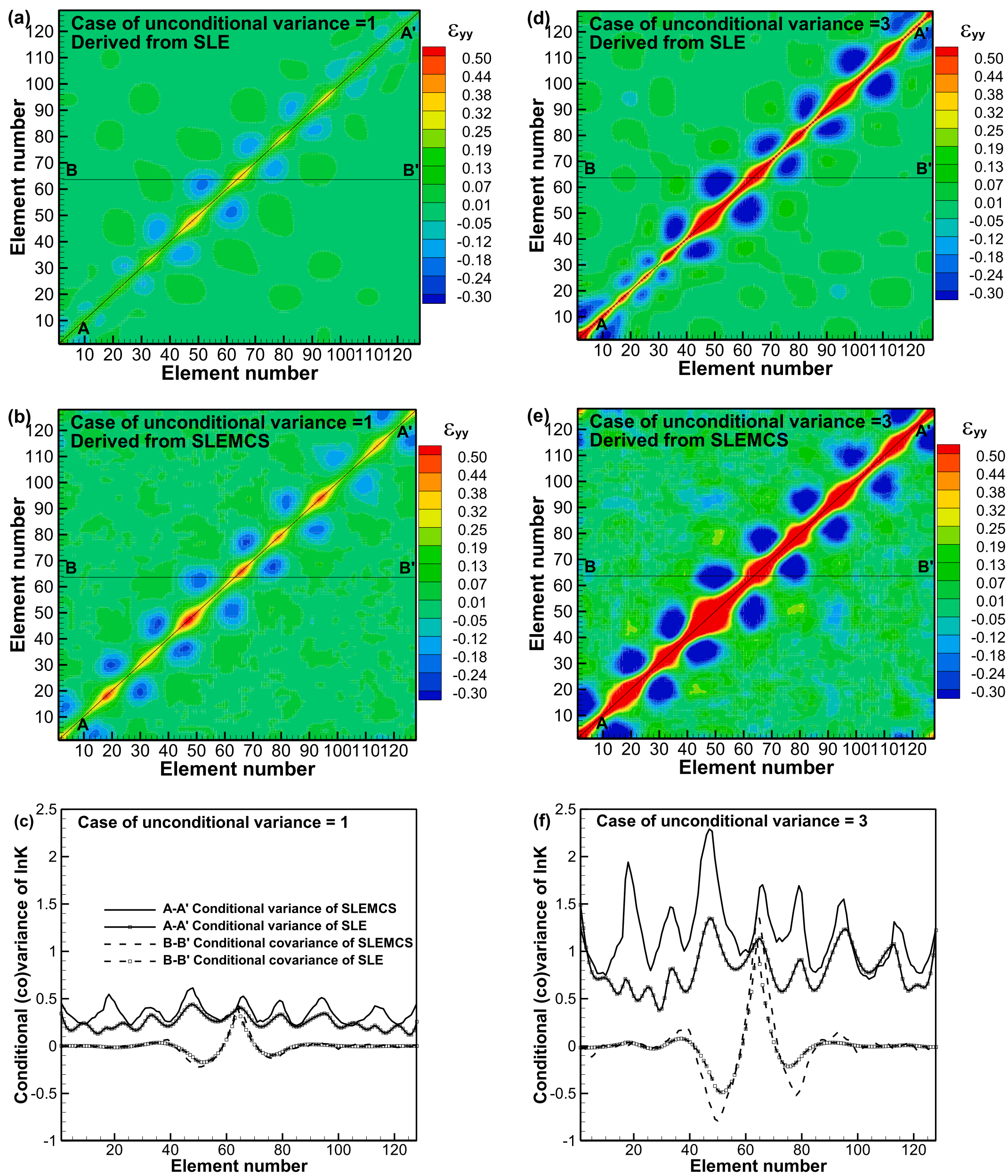

Fig. 9. Comparisons of the conditional covariance of ln$K$ from SLE and SLEMCS for the Var_ln$K$ = 1.0 (a, b, and c) or 3.0 (d, e, and f). c and f are plots of covariance along the cross-sections A-A' and B-B'.

Table 1
The CPU time-demanding for generate 2000 conditional realizations by different MC methods and directly generate effective K field by SLE.

Methods	Case of 1D HT for unconditional variance of ln$K$ = 1.0	Case of 1D HT for unconditional variance of ln$K$ = 3.0	Case of 2D HT
SLEMCS	182.334	228.719	499.554
SLEKLM	3.281	3.470	39.741
SLE	0.0349	0.585	0.2778

*Unit: minutes; CPU: Intel(R) Xeon(R) W-2133 @3.6 GHz; RAM: 32.0 GB.

approximation of the conditional covariance matrix of ln$K$ (Eq. (19)) at the last iteration is used as the conditional covariance. On the other hand, the conditional covariance matrix for the SLEMCS approach is derived from a statistical covariance analysis of the 2,000 conditional realizations. The covariance matrices for cases with the unconditional variance of ln$K$ of 1.0 from SLE and SLEMCS are displayed in Fig. 9a and b, respectively. Fig. 9d and e show the corresponding covariances for the unconditional variance of ln$K$ of 3.0.

The patterns of these two conditional covariance matrices are similar, although the values from SLEMCS are larger than those from SLE. The difference increases with the unconditional variance of ln$K$ (Fig. 9c and f). The largest conditional variance of ln$K$ (diagonal elements of the matrices) is at the location of head measurement, while the minimum is at the location between the head observed locations. That is, the head data at the observation wells reduce the uncertainty of the ln$K$ between the observation wells but not that at the observation well. Such

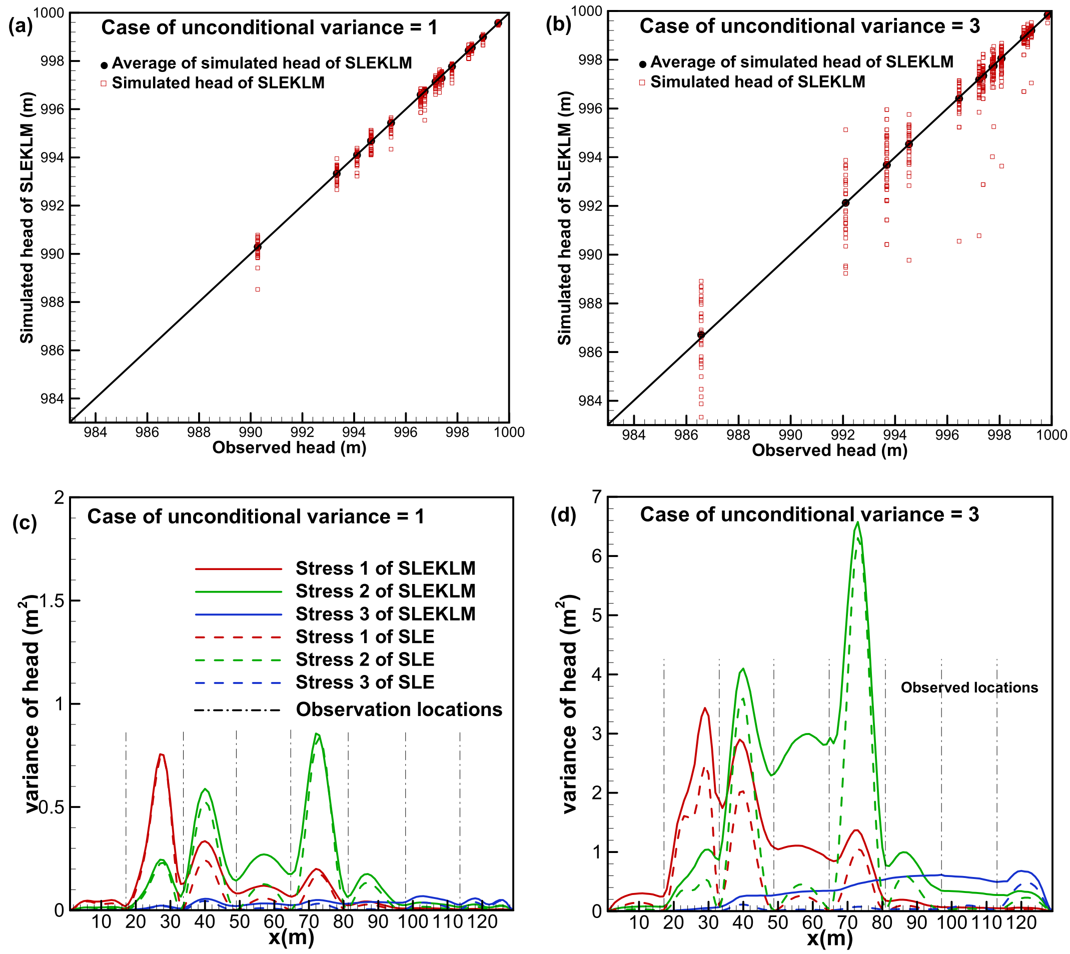

Fig. 10. Simulated head of SLEKLM versus observation head for three stresses for: (a) Var_ln$K$ = 1 and (b) Var_ln$K$ = 3; Comparisons of conditional variance of the head using first-order analysis in SLE (the dashed lines) with the conditional variance of the head by SLEKLM method for three stresses for: (c) Var_ln$K$ = 1 and (d) Var_ln$K$ = 3.

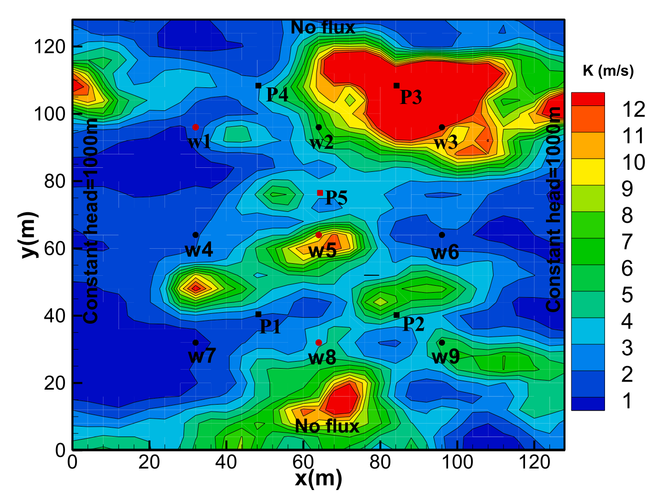

Fig. 11. The true conductivity field of the two-dimensional horizontal confined aquifer. The black dots denote observation wells and the red dots represent the pumping wells w1, w5, and w8, for the three stresses of the HT survey.

behavior is distinctly different from the conditional variance resulted from conditioning with ln$K$ measurements (Fig. 3b), where the conditional variance is zero at the measurement locations. Such findings are consistent with the explanation of the impacts of head measurements of HT by Yeh et al. (2014). Notice that the variance is always positive, but the covariance can be negative.

4.2.2. SLEKLM

SLEMCS evaluation is computationally intensive since it requires to run SLE 2,000 times using 2,000 random realizations as initial fields. A new approach (i.e., SLEKLM) is proposed. Specifically, it first employs SLE to derive the conditional effective ln$K$ field and conditional covariance matrix of ln$K$. Using the conditional covariance of ln$K$ resulting from SLE, SLEKLM then generates the zero mean conditional realizations. Afterward, these zero mean realizations are added to the conditional effective ln$K$ field to form the conditional realizations of ln$K$ fields, which are then converted to the conditional realizations of K fields.

A comparison of the efficiency of the two methods of SLEMCS and SLEKLM is shown in Table 1. Using SLEKLM method takes only a few tenths of the computational-time of SLEMCS, while the CPU time required by SLE is much less than those of the SLEMCS and SLEKLM, since SLE directly derives the conditional effective K field and associated conditional covariance matrix.

Next, we investigate whether these conditional random fields derived from SLEKLM honor the observed heads at the observed locations during the HT survey. For this purpose, we use these conditional random fields (2,000 realizations) to simulate the HT survey. In Fig. 10a and b, we plot the simulated heads at the observation wells of each pumping test against those heads simulated using the true K field (observed true heads). These plots show that the simulated heads agree with the observed heads only in an average sense: they scatter around

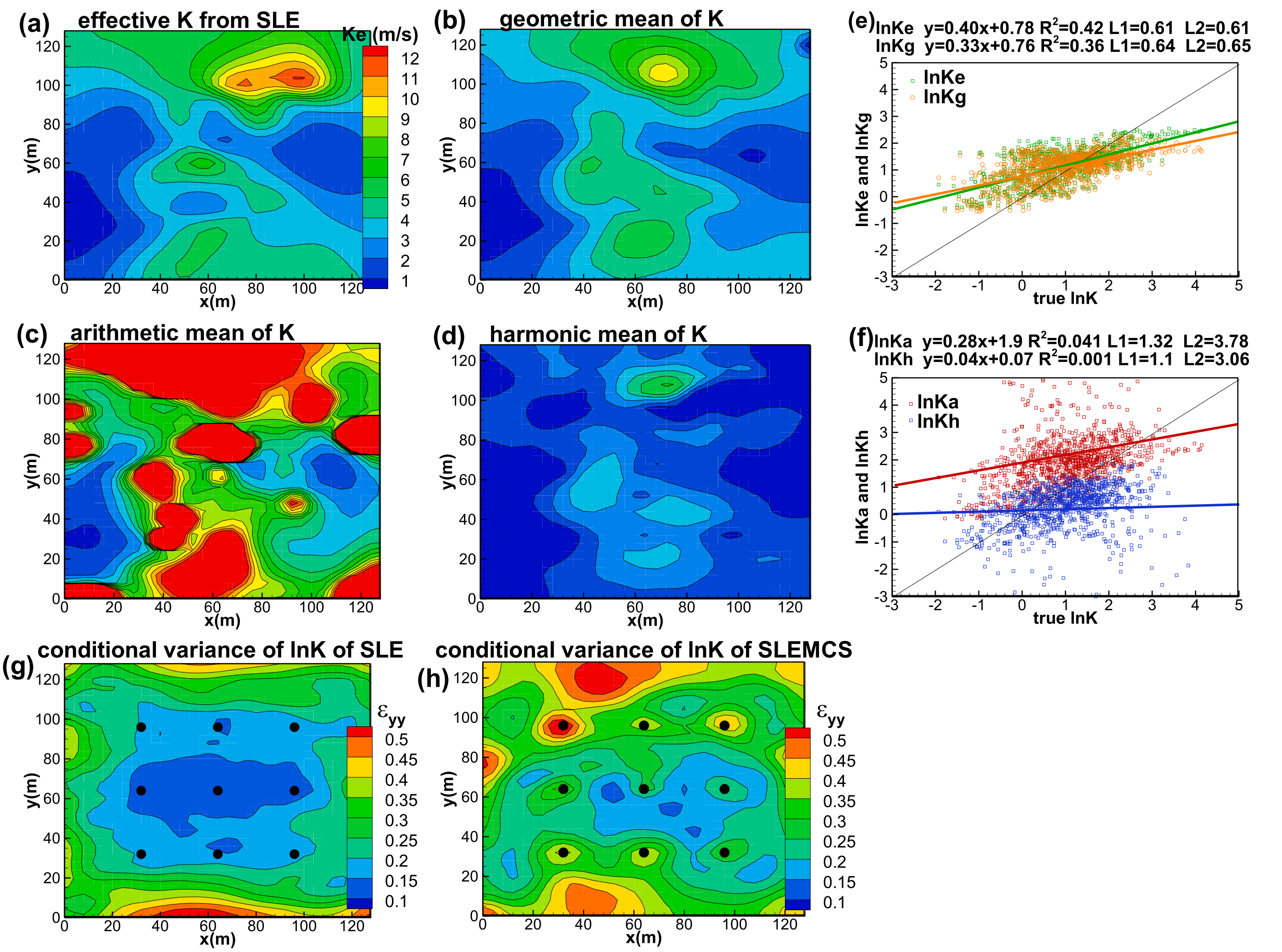

Fig. 12. Contour plots of (a) the effective K from SLE; (b), (c), and (d) the geometric, the arithmetic, the harmonic mean of the SLEMC. Scatter plots of (e) the true ln$K$ field vs. the effective and the geometric mean of ln$K$ field; (f) the true ln$K$ field vs. the arithmetic mean and the harmonic mean of SLEMC. The conditional variance of ln$K$ from: (g) SLE and (h) SLEMCS.

the one-to-one line.

The conditional variances of the heads from SLEKLM for different pumping stresses of HT are illustrated in Fig. 10c and d. The head variances at the observation locations are nonzero, even though they are much smaller than those at other locations, manifesting the effects of head conditioning. In other words, SLEKLM does not guarantee the preservation of the head measurements. Preservation of the observed heads can only be accomplished via solving the governing flow equation, rather than generating them from the conditional covariance.

5. Two-dimensional numerical experiments

Reference field. Here, a two-dimensional heterogeneous aquifer with a dimension of 128 m × 128 m is discretized into 1024 (4 m × 4 m) elements. Each element is assigned a K value using the FFT random field generator. The generated K field (see Fig. 11) (i.e., the true or reference field) has the unconditional mean and variance of ln$K$ of 1.0 and an exponential correlation structure with anisotropic correlation scales ($\lambda_x = 40$m and $\lambda_y = 20$m in × and y directions, respectively). The upper and lower sides of the aquifer are no-flow boundaries, and the left and right sides are constant head boundaries of 1000 m. Nine wells (w1 to w9) are installed, and three pumping stresses are conduct at w1, w5, and w8 for HT survey. Each stress is a constant discharge ($Q = 0.05m^3/s$) at one of the wells, and VSAFT2 simulates the steady-state flow. The simulated heads at the other eight wells are collected for each stress. Subsequently, a total of 24 head measurements for the three tests are simultaneously used for inversion using SLE, SLEMCS, and SLEKLM approach without using any K measurement.

Conditional K fields. The effective hydraulic conductivity from SLE is displayed in Fig. 12a. With the same head measurements, we use SLEMCS to derive 2,000 conditional K realizations that honor the observed heads. The geometric, arithmetic, and harmonic averages of these realizations are depicted in Fig. 12b-d, respectively. The scatter plot comparing the true and effective K, and the geometric average from SLEMCS is in Fig. 12e. The scatter plot for the arithmetic, and harmonic averages of SLEMCS vs. the true field is in Fig. 12f.

From Fig. 12a and b, we notice that the effective K from SLE is similar to the geometric mean of the K fields from SLEMCS; both are all unbiased with the true field (Fig. 12e). The field from the arithmetic mean of the SLEMCS generally is larger than the true field, while that from the harmonic mean is smaller, as shown in Fig. 12f.

The patterns of the conditional variance of ln$K$ from SLE and SLEMCS (Fig. 12g and h, respectively) are similar, but the values from SLEMCS are larger than those from SLE. Both yield small uncertainty of the estimated ln$K$ near the observation positions and significant uncertainty far away from the observation ports, especially near the boundary, consistent with those in one-dimensional results.

Conditional head Fields. We use the same procedure as in the 1-D case to derive the conditional head fields. To check if the conditional head fields honor the observed heads, we subtract the conditional head field obtained by the three approaches from the true head field, and then take its absolute value to obtain the Fig. 13a-c (only stress 1 is

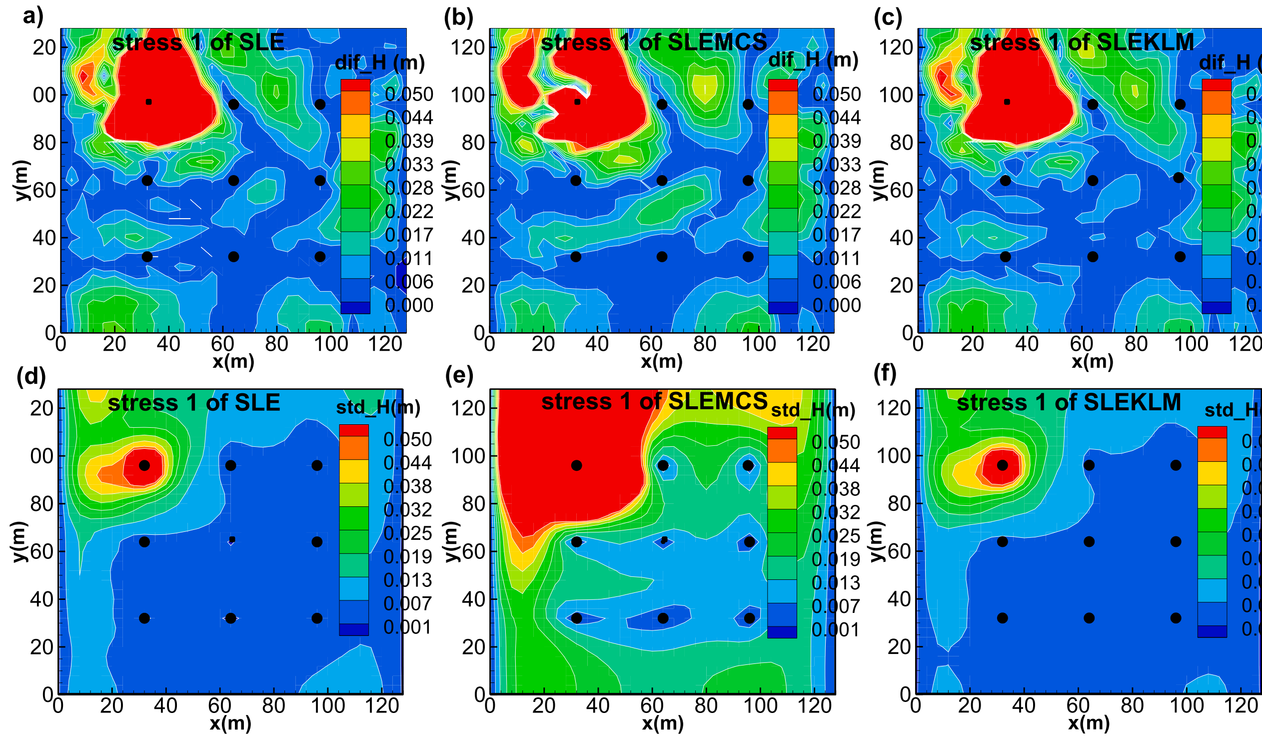

Fig. 13. The absolute value of the difference between the true head field and (a) the simulated head field based on K_e; (b) the average head derived from SLEMCS; (c) the average head derived from SLEKLM of stress 1. The conditional head standard deviation of stress 1 from (d) the first-order analysis in SLE, (e) the SLEMCS simulations, and (f) those from the SLEKLM simulations.

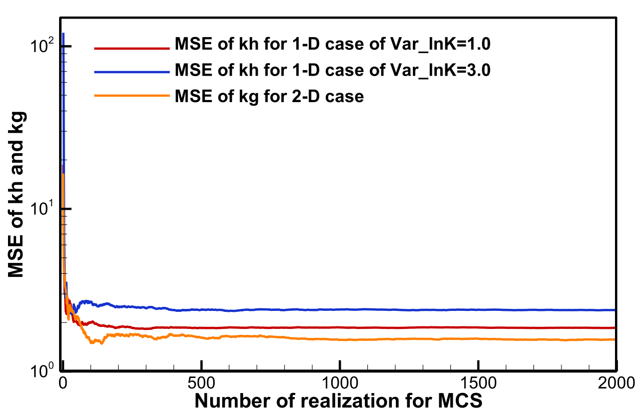

Fig. 14. MSE of harmonic mean (K_h) for 1-D HT cases and geometric mean (K_g) for 2-D HT case.

shown). The simulated head, based on the effective K, the average head from SLEMCS, and that from SLEKLM honor the head observations.

Conditional head standard deviation from SLEMCS are generally larger than those from the SLE and SLEKLM as shown in Fig. 13d-f. Although the standard deviation of the head field from the SLEKLM at the observation wells is not zero, the pattern is similar to those from the SLE and SLEMCS approach.

6. Effect of ensemble size for MCS

To ensure our MCS results from the limited domain size are conclusive, we investigate the effect of the number of realizations on the ensemble harmonic and the geometric mean of K from SLEMCS in comparison with the effective K from SLE using the mean square error as a criterion:

$$MSE = \frac{1}{N}\sum_{i=1}^{N}(Z_i - Z_i')^2 \tag{20}$$

This MSE measures the difference between Z_i (the effective conductivity from SLE) and Z_i' (the ensemble harmonic or geometric mean of hydraulic conductivity from SLEMCS); N is the total number of elements. If the MSE value is small, then the averages of the SLEMCS is equivalent to the effective K.

As shown in Fig. 14, for 1-D aquifers with the variance of ln$K$ of 1 and 3, the MSE value of the harmonic mean of SLEMCS (K_h) drops rapidly to a minimal value, and it stabilizes after about 500 realizations. For 2-D aquifers, the geometric mean of the SLEMCS (K_g) also behaves similarly.

7. Demonstration of the usefulness of the approaches

To demonstrate the utility of the SLE, SLEMCS, and SLEKLM, we used their estimated K fields to predict an independent pumping test using wells, not used in the previous HT analysis. The independent pumping test experiment uses the same grid size and boundary condition as the 2-D HT experiment but uses different the pumping and observation well locations, i.e., the pumping well P5 with a constant discharge (Q = 0.2m^3/s) and the observation wells, P1, P2, P3, and P4 as shown in Fig. 11. The specific storage (0.02/m) is known and uniform over the aquifer. The initial head is 1000 m at all nodes and equal to the left and right boundary conditions. We then simulate transient drawdown behaviors induced by this pumping based on the true and the estimated K fields from the previous HT analysis from the three different methods.

The drawdown distribution at the steady-state of the true K field is displayed in Fig. 15a, while Fig. 15b presents the simulated drawdown distribution using the conditional effective K derived from SLE. Meanwhile, the average of 1,000 realizations of simulated drawdown fields using 1,000 conditional realizations of K fields derived from SLEMCS and SLEKLM are presented in Fig. 15c and d, respectively.

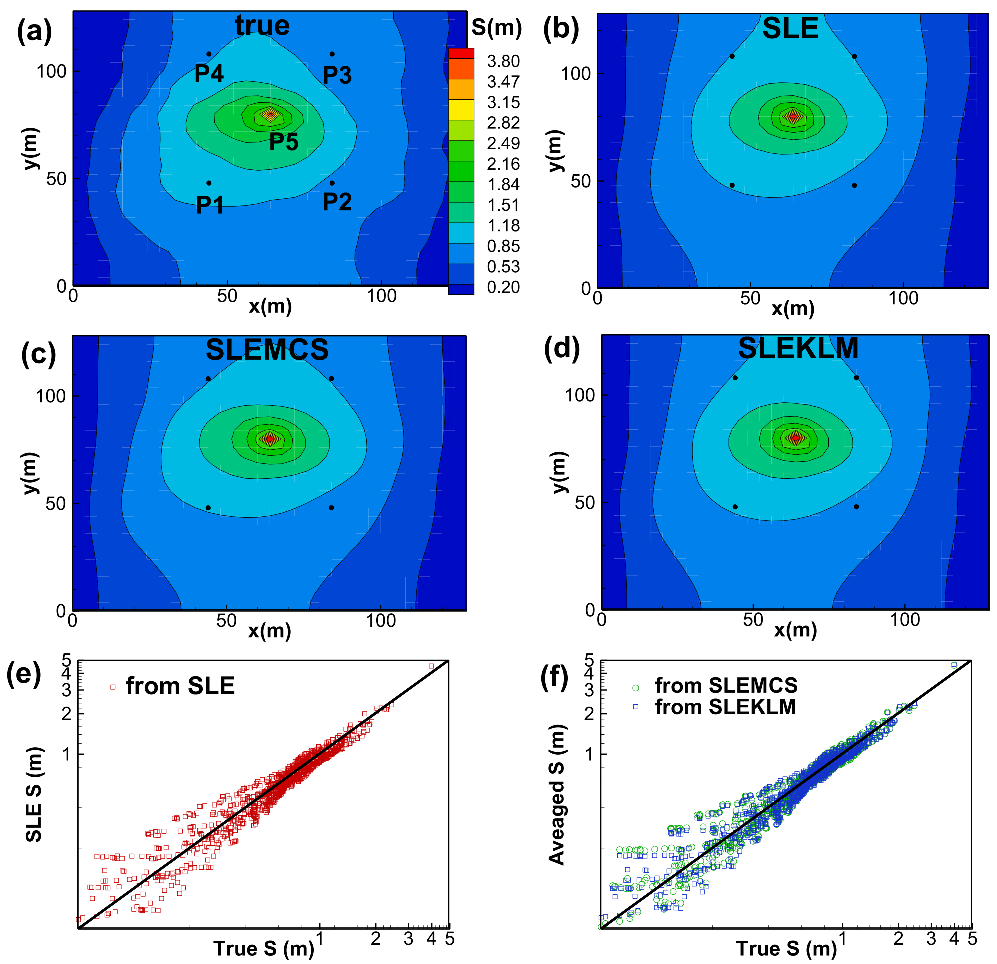

Fig. 15. The contour maps of the drawdown (S) at the steady state (i.e., t = 80 s) derived from (a) true K field; (b) the effective K field; (c) and (d) the conditional realizations of SLEMCS and SLEKLM, respectively. The scatter plot of drawdown between (e) the true and effective K field; (f) the true and SLEMCS or SLEKLM.

The comparisons between the true and the simulated drawdowns using the conditional effective K over the entire aquifer is illustrated in Fig. 15e as the scatter plot. The scatter plot of the averaged drawdowns from SLEMCS and SLEKLM vs. the true is presented in Fig. 15f. Overall, the effective K from SLE yields unbiased predictions of the drawdown. Likewise, the average of the simulated drawdowns from SLEMCS and SLEKLM also are unbiased. Notice large scatterings at small drawdown values in these scatter plots are attributed to the sparse well network used in the HT survey and log-scale plot.

Lastly, the usefulness of the Monte Carlo simulations using SLEMCS and SLEKLM for showing the uncertainty of the drawdown at the observation well P1 and P3 are illustrated in Fig. 16. In all these drawdown-time plots, the solid black lines are the drawdown curves in the true field, while the light blue lines are the 1,000 possible drawdown-time curves simulated by the SLEMCS and SLEKLM. As we have remarked before, the SLEKLM likely underestimates the conditional variance of ln$K$. As such, it produces narrow bands of possible drawdown-time behaviors. Besides, the results in Fig. 16 also reveals that the unbiased predictions shown in Fig. 15 do not apply to observed heads at one or two locations.

8. Summary and conclusion

To explain conditional mean, effective, and realizations of conductivity fields, we develop conditional Monte Carlo simulation algorithms using hydraulic conductivity measurements (namely, KSA and KLM) or based on hydraulic head measurements from the hydraulic tomographic survey (SLEMCS and SLEKLM).

Results of the analysis of these algorithms can be summarized as follows:

1. KSA and KLM can generate conditional realizations, which have the same spatial statistics as the unconditional K field. Also, they yield conditional mean and covariance, which are the same as the kriging mean and conditional covariance.
2. Interpretation of HT data using SLE yields a conditional effective hydraulic conductivity field and the conditional covariance of the estimated field, given the head, discharge, and boundary information during the HT survey. On the other hand, SLEMCS produce conditional realizations (equally likely hydraulic conductivity fields) that honor the observed heads during HT surveys and are as jagged as the true field. The conditional effective hydraulic conductivity of SLE is close to the harmonic average of all these realizations for one-dimensional flow but agrees with the geometric average for two-dimensional flow. The covariance functions of these realizations from SLEMCS are similar in pattern with that of the conditional covariance function of SLE, although the values from SLEMCS are larger than those from SLE, and the deviation increases with the unconditional variance of ln$K$.
3. SLEKLM can efficiently generate conditional realizations of hydraulic conductivity fields by taking advantage of SLE's conditional effective hydraulic conductivity field and conditional covariance function. However, the simulated heads from the generated conditional realizations of K match the observed head data of HT survey only in the average sense.
4. Applications of SLE, SLEMCS, and SLEKLM to an independent flow

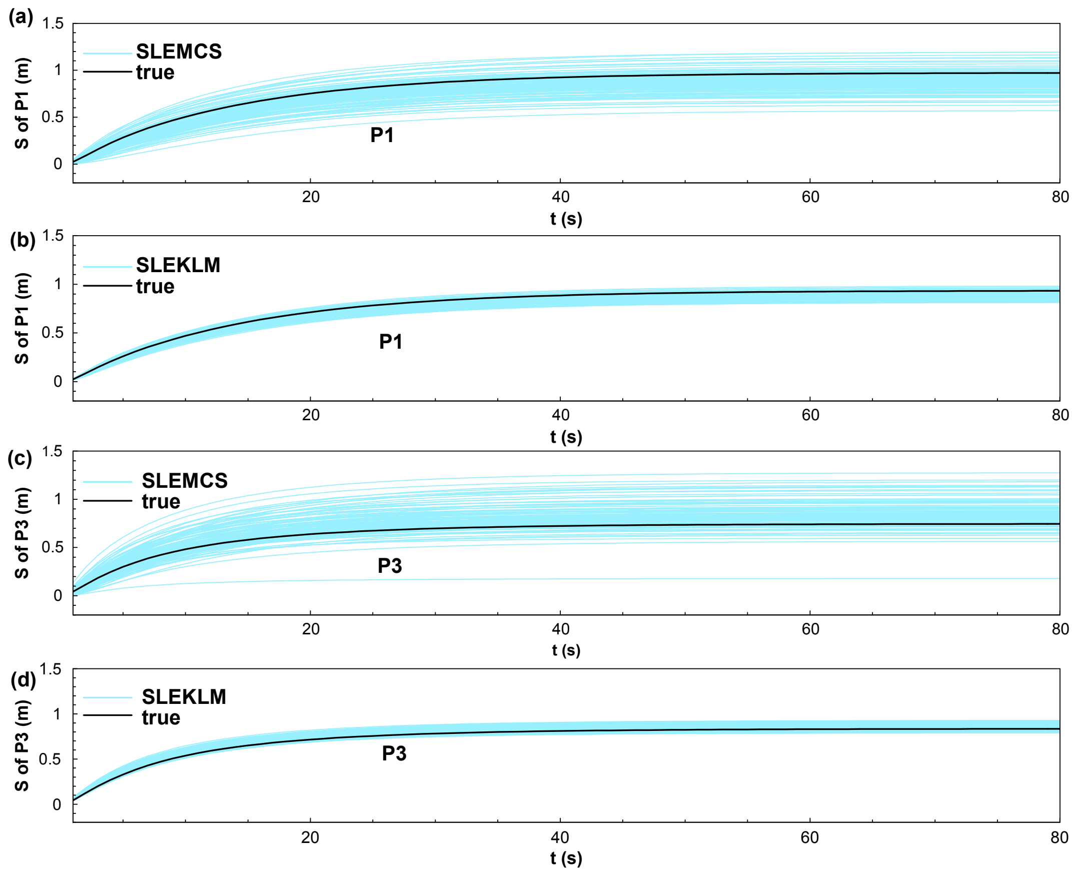

Fig. 16. The drawdown curves at observation P1 and P3 derived from conditional realizations of SLEMCS and SLEKLM. The locations of P1 and P3 are shown in Fig. 11.

event demonstrate that all approaches yield unbiased prediction of the true head field, and the uncertainty of drawdown around the observed locations from SLEKLM are small.

Based on these results, we come to the following conclusions:

1. The effects of conditioning using K and head measurements are different.
2. Harmonic and geometric averages of conditional hydraulic conductivity realizations are equivalent to the effective hydraulic conductivity derived from SLE for one- and two-dimensional flow problems, respectively.
3. The effective hydraulic conductivity from HT can predict head fields that are unbiased and preserve the observed heads during each HT pumping test. It also yields an unbiased prediction of the head field under a different flow scenario.
4. While SLEKLM is more computationally efficient than SLEMCS, but its conditional variance is smaller than that of SLEMCS. On the other hand, SLE and a first-order analysis is a computationally efficient approach for the same purpose but derives only conditional variances, without the generation of conditional realizations.

Lastly, as stated in Yeh et al. (2015), the uncertainty analysis is not to seek absolute uncertainty but to gauge the relative uncertainty between different operational strategies. Therefore, we recommend the use of SLE or SLEKLM for practical applications, due to their computational efficiency. Moreover, if we just estimate the head and its uncertainty, we recommend the SLE method since it can directly derive the best-unbiased K estimates honoring the observations and the conditional covariance addressing the uncertainty of estimates, and it also avoids the MC intensive computational efforts. However, if we need to estimate the uncertainty of flow and concentration fields and derive possible realizations, we suggest the conditional realizations from SLEMCS and SLEKLM.

CRediT authorship contribution statement

Xu Gao: Conceptualization, Formal analysis, Writing - original draft. **Tian-Chyi Jim Yeh:** Methodology, Software, Writing - review & editing. **E-Chuan Yan:** Validation, Supervision. **Yu-Li Wang:** Software, Visualization. **Yonghong Hao:** Supervision.

Declaration of Competing Interest

The authors declare that they have no known competing financial interests or personal relationships that could have appeared to influence the work reported in this paper.

Acknowledgments

The first author gratefully acknowledges financial support by China Scholarship Council (CSC, No.201606410033) and the Fundamental Research Funds for the Central Universities, China University of Geosciences (Wuhan) (Grant No. CUG200612) and the Laboratory Open Project Fund of Engineering Research Center of Rock-Soil Drilling & Excavation and Protection, Ministry of Education (Grant No. 202002). The third authors acknowledge the support by the National Natural Science Foundation of China (Grant No.41172282 and No. 41672313). The corresponding author acknowledges the partially supported by the U.S. NSF grant EAR1931756.

References

Bohling, G.C., Zhan, X., Butler, J.J., Zheng, L., 2002. Steady shape analysis of tomographic pumping tests for characterization of aquifer heterogeneities. Water Resour. Res. 38 (12).

Brauchler, R., Cheng, J.-T., Dietrich, P., Everett, M., Johnson, B., Liedl, R., Sauter, M., 2007. An inversion strategy for hydraulic tomography: coupling travel time and amplitude inversion. J. Hydrol. 345 (3), 184–198.

Brauchler, R., Liedl, R., Dietrich, P., 2003. A travel time based hydraulic tomographic approach. Water Resour. Res. 39 (12).

Cardiff, M., Barrash, W., 2011. 3-D transient hydraulic tomography in unconfined aquifers with fast drainage response. Water Resour. Res. 47 (12).

Cardiff, M., Barrash, W., Kitanidis, P.K., 2013. Hydraulic conductivity imaging from 3-D transient hydraulic tomography at several pumping/observation densities. Water Resour. Res. 49 (11), 7311–7326.

Castagna, M., Bellin, A., 2009. A Bayesian approach for inversion of hydraulic tomographic data. Water Resour. Res. 45 (4).

Fienen, M.N., Clemo, T., Kitanidis, P.K., 2008. An interactive Bayesian geostatistical inverse protocol for hydraulic tomography. Water Resour. Res. 44 (12).

Franssen, H.J.H., Alcolea, A., Riva, M., Bakr, M., Wiel, N.V., DerF, S., Guadagnini, A., 2009. A comparison of seven methods for the inverse modelling of groundwater flow. application to the characterisation of well catchments. Adv. Water Resour. 32 (6), 851–872.

Gelhar, Lynn W., 1986. Stochastic subsurface hydrology from theory to applications. Water Resour. Res. 22 (9S), 135S–145S.

Gottlieb, J., Dietrich, P., 1995. Identification of the permeability distribution in soil by hydraulic tomography. Inverse Prob. 11 (2), 353.

Gutjahr, A., Bullard, B., Hatch, S., Hughson, L., 1994. Joint conditional simulations and the spectral approach for flow modeling. Stochastic Hydrol. Hydraul. 8 (1), 79–108.

Gutjahr, A.L., 1989. Fast Fourier Transforms for Random Field Generation: Project Report for Los Alamos Grant to New Mexico Tech. New Mexico Institute of Mining and Technology.

Hanna, S., Yeh, T.-C.J., 1998. Estimation of co-conditional moments of transmissivity, hydraulic head, and velocity fields. Adv. Water Resour. 22 (1), 87–95.

Hochstetler, D.L., Barrash, W., Leven, C., Cardiff, M., Chidichimo, F., Kitanidis, P.K., 2016. Hydraulic tomography: continuity and discontinuity of high-K and low-K zones. Groundwater 54 (2), 171–185.

Illman, W.A., Liu, X., Craig, A., 2007. Steady-state hydraulic tomography in a laboratory aquifer with deterministic heterogeneity: multi-method and multiscale validation of hydraulic conductivity tomograms. J. Hydrol. 341 (3), 222–234.

Illman, W.A., Liu, X., Takeuchi, S., Yeh, T.-C.J., Ando, K., Saegusa, H., 2009. Hydraulic tomography in fractured granite: Mizunami Underground Research site, Japan. Water Resour. Res. 45 (1).

Lavenue, M., Marsily, G., 2001. Three-dimensional interference test interpretation in a fractured aquifer using the pilot point inverse method. Water Resour. Res. 37 (11), 2659–2675.

Liu, S., Yeh, T.-C.J., Gardiner, R., 2002. Effectiveness of hydraulic tomography: sandbox experiments. Water Resour. Res. 38 (4).

Liu, X., Illman, W.A., Craig, A.J., Zhu, J., Yeh, T.-C.J, 2007. Laboratory sandbox validation of transient hydraulic tomography. Water Resour. Res. 43 (5).

Liu, X., Kitanidis, P.K., 2011. Large-scale inverse modeling with an application in hydraulic tomography. Water Resour. Res. 47 (2).

Lu, Z., Zhang, D., 2004. Conditional simulations of flow in randomly heterogeneous porous media using a KL-based moment-equation approach. Adv. Water Resour. 27 (9), 859–874.

Ma, J., Dong, Z.Y., Zhang, P., 2006. Comparison of BR and QR eigenvalue algorithms for power system small signal stability analysis. IEEE Trans. Power Syst. 21 (4), 1848–1855.

MathWorks, I. (2005). MATLAB: the language of technical computing. Desktop tools and development environment, version 7 (Vol. 9). MathWorks.

Ni, C.-F., Yeh, T.-C.J., 2008. Stochastic inversion of pneumatic cross-hole tests and barometric pressure fluctuations in heterogeneous unsaturated formations. Adv. Water Resour. 31 (12), 1708–1718.

Nowak, W., 2009. Best unbiased ensemble linearization and the quasi-linear Kalman ensemble generator. Water Resour. Res. 45 (4).

Indelman, Peter, 2003. Transient pumping well flow in weakly heterogeneous formations. Water Resour. Res. 39 (10), 321–325.

Kitanidis, P.K., 1995. Quasi-linear geostatistical theory for inversing. Water Resour. Res. 31 (10), 2411–2419.

Kitanidis, P.K., 1997. Introduction to geostatistics: applications in hydrogeology. Cambridge University Press.

Sanchez-León, E., Leven, C., Haslauer, C.P., Cirpka, O.A., 2016. Combining 3D hydraulic tomography with tracer tests for improved transport characterization. Groundwater 54 (4), 498–507.

Schöniger, A., Nowak, W., Hendricks Franssen, H., 2012. Parameter estimation by ensemble Kalman filters with transformed data: Approach and application to hydraulic tomography. Water Resour. Res. 48 (4).

Tosaka, H., Masumoto, K., Kojima, K., 1993. Hydropulse tomography for identifying 3-D permeability distribution. High Level Radioactive Waste Manage.: Proc. 1.

Vasco, D.W., Karasaki, K., 2006. Interpretation and inversion of low-frequency head observations. Water Resour. Res. 42 (5).

Xiang, J., Yeh, T.-C.J., Lee, C., Hsu, K., Wen, J., 2009. A simultaneous successive linear estimator and a guide for hydraulic tomography analysis. Water Resour. Res. 45 (2).

Yaz, E. E., & Azemi, A. (1995). Utilizing MATLAB in two graduate electrical engineering courses. Frontiers in Education Conference, 1995. Proceedings., 1995, 1, 2c6–1.

Yeh, T.-C.J., 1992. Stochastic modelling of groundwater flow and solute transport in aquifers. Hydrol. Process. 6 (4), 369–395.

Yeh, T.-C.J., Gutjahr, A.L., Jin, M., 1995. An iterative cokriging-like technique for groundwater flow modeling. Groundwater 33 (1), 33–41.

Yeh, T.-C.J., Jin, M., Hanna, S., 1996. An iterative stochastic inverse method: Conditional effective transmissivity and hydraulic head fields. Water Resour. Res. 32 (1), 85–92.

Yeh, T.-C.J., Mao, D., Zha, Y., Hsu, K., Lee, C., Wen, J., Lu, W., Yang, J., 2014. Why hydraulic tomography works? Groundwater 52 (2), 168–172.

Yeh, T.-C.J., Srivastava, R., Guzman, A., Harter, T., 1993. A numerical model for water flow and chemical transport in variably saturated porous media. Ground Water 31 (4), 634–644. https://doi.org/10.1111/j.1745-6584.1993.tb00597.x.

Yeh, T.-C.J., Liu, S., 2000. Hydraulic tomography: development of a new aquifer test method. Water Resour. Res. 36 (8), 2095–2105. https://doi.org/10.1029/2000WR900114.

Yeh, T.-C.J., Khaleel, R., Carroll, K.C., 2015. Flow through Heterogeneous Geologic Media. Cambridge University Press.

Yin, D., Illman, W.A., 2009. Hydraulic tomography using temporal moments of drawdown recovery data: a laboratory sandbox study. Water Resour. Res. 45 (1).

Zhu, J., Yeh, T.-C.J., 2006. Analysis of hydraulic tomography using temporal moments of drawdown recovery data. Water Resour. Res. 42 (2).

Zhu, J., Yeh, T.-C.J., 2005. Characterization of aquifer heterogeneity using transient hydraulic tomography. Water Resour. Res. 41 (7).